WORLD CONFERENCE ON TIMBER ENGINEERING 2025
BRISBANE, AUSTRALIA
Advancing Timber for the Future Built Environment

MOMENT RESISTANT CONNECTIONS WITH GLUED-IN-RODS IN GLUELAM

W.H. de Groot[1], K.E.M. Raymakers[2], S.P.G. Moonen[3], N. Castelein[4]

ABSTRACT: This paper reports an experimental and theoretical study of moment resistant connections with glued-in-rods. For road sign structures in the Netherlands timber portal frames are developed made of gluelam elements with a span of approximately 20 meters. Due to limited space the columns are designed moment rigid connected to the foundation. Twenty Glued-in-Rods (M16-8.8) are used to connect the timber hollow square tube moment rigid to the steel foundation.

To achieve calculation rules for this connection, the author developed a prediction model that describes the moment capacity and rotational stiffness of a square timber cross-section using up to three layers of Glued-in-Rods in the tensile zone. Additionally, several experimental tests were conducted to obtain parameters as input for the analytical model. Different experiments were then performed and the results compared to the prediction models. These results show that the model predicts the strength of the connection with accuracy, however the stiffness model [21] overestimates the rotational stiffness of the connection. This disparity could be caused by local imperfections and the stiffness of the connector. Results also show that the failure mechanism is as designed and predicted. Further research is needed to incorporate the effects of moisture levels on the strength of this connection and to refine the stiffness prediction.

KEYWORDS: Glued-in-rods, Cross-sectional mechanics, Prediction model, Connection failure, etc

1 – INTRODUCTION

The use of timber within building projects is becoming more popular since the material is seen as a step towards a more sustainable future [28], [7], [9]. Timber is lightweight, has a good strength-to-weight ratio [20], and stores CO_2. The Eurocode 5 [16] has extensive information regarding the design capacity of dowelled connections and mechanical fasteners. An alternative for a dowelled connection is the Glued-in-Rod connection (GiR); this connection has, however very few design guidelines compared to the doweled type and is currently not present in Eurocode 5 [16]. The GiR connection consist of a rod, adhesive, and timber, where the timber has a pre-drilled hole into which the rod is glued. The hole is drilled either parallel or perpendicular to the grain, it can also be drilled at an angle [4]. The GiR field has been around since the 1980s, [13], and since then, there has been done ample research done into the pull-out behavior [22], [2], [26], [24], [23], [12], [14], which mostly investigated the load-slip behavior. Beside this load-slip behaviour, geometrical parameters and their influence on the failure behaviour such as rod diameters and edge distances [26], [14], [27] are significant. The current research [21] focuses on the material behavior of single rods [27] or the cyclic behavior of GiR [18], [11], [19], the starting point of said research can be found in some books such as the Step1995 [25]. The methods and results presented here aim to provide the designer with new tools to utilize GiR connection by analytically predicting the ultimate moment capacity and rotational stiffness for a hollow rectangular cross-section. The outcome of this model is verified using an experimental study. The material non-homogeneity of the connection and the number of options for material choices has made it difficult to come to any conclusive design standard. GiR connection remains interesting for designers and does have benefits with the increasing use of timber within structures. The connection itself is aesthetically pleasing due to the connection itself being covered by timber. This also leads to an increased fire resistance [27], [8], showing that this connection has multiple practical benefits.

[1]Eindhoven University of Technology, P.O. Box 513, 5600 MB Eindhoven, The Netherlands and SHR Timber Research, Nieuwe Kanaal 9E, 6709 PA Wageningen, The Netherlands, w.h.d.groot@tue.nl
[2]Adviesbureau Van de Laar, Zwaanstraat 31R, 5651 CA Eindhoven, The Netherlands, karsraymakers@gmail.com
[3]Eindhoven University of Technology, P.O. Box 513, 5600 MB Eindhoven, S.P.G.Moonen@tue.nl
[4]Niels Castelein, Sweco, De Holle Bilt 22, 3732 HM De Bilt, The Netherlands, niels.castelein@sweco.nl

2 – THEORETICAL BACKGROUND

2.1 LOAD SITUATION AND MECHANICAL SCHEME

To research a GiR column-base connection, a road sign portal frame is analyzed. The portal frame found in Naaldwijk, The Netherlands, is used as a reference and starting point.

In this GiR column-base connection it is first considered that a wind load acts out of plane on a portal frame. This can be redrawn to an inclined column with a horizontal load on top. These loads cause the situation displayed in Figure 2.

The GiR connection is modeled as a rotational spring due to the connection not being considered as completely

https://doi.org/10.52202/080513-0180

Figure 1: Road sign portal frame, Naaldwijk, The Netherlands

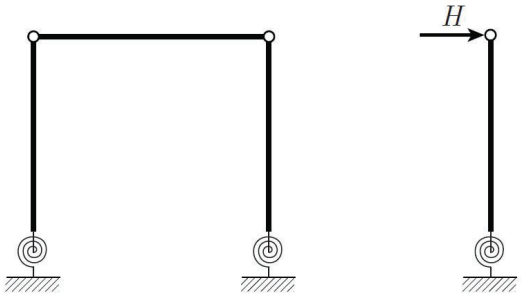

Figure 2: Out of plane loading of portal frame

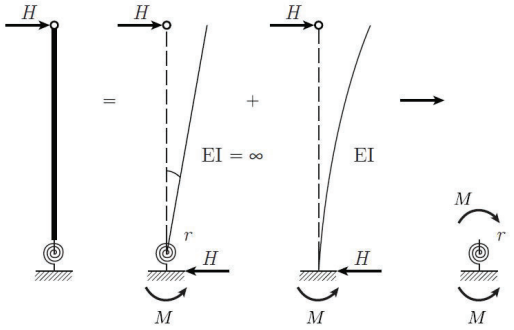

Figure 3: Mechanical scheme, modelling the GiR connection as a rotational spring

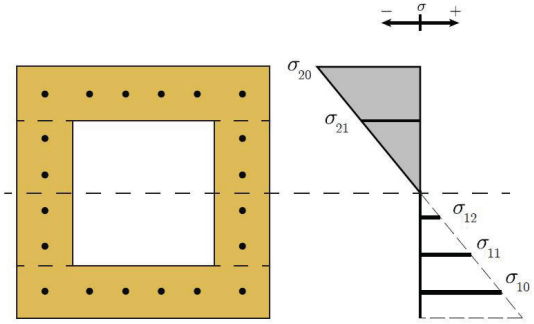

Figure 4: Stress distribution of a GiR connection

moment rigid, while the horizontal load results in a moment, the rotation spring has a certain capacity which is related to the moment over the rotation.

When following this mechanical scheme, a rotational effect occurs, this rotation enables a further in-depth exploration of the stress distribution and possible failure mechanisms of this connection under the current loading arrangement. The rotational spring stiffness of said connection has to be determined through analytical means and experimental measurements. Since the connection is prevented from rotating freely due to being mounted on a flat steel surface, the timber is considered in compression while the steel glued-in-rods are in tension. The material behaviour is considered parallel to the grain. This type of situation adds certain failure mechanisms which have to be considered. In figure 4 a stress distribution of the example in Naaldwijk mentioned is displayed which shows that one side is in compression, for this the timber itself has the largest area, therefore it is assumed that the steel rod surface is negligible in comparison. The other side is in tension, in which the steel rods are considered the critical element in this load situation, since the timber is not connected to the steel plate.

The accompanying failure mechanisms are considered in subsections 2.4 and 2.5.

2.2 BENDING BEHAVIOR OF GLUED-IN-ROD CONNECTIONS

The bending moment that is applied within this load situation seen in Figure 3 is deconstructed into an internal compressive and tensile force of which a stress diagram is seen in Figure 4. In a symmetrical cross-section the neutral axis and point of rotation are located in the center. Some studies have used this principle to create a prediction model [15] or to create a vertical gap between the connection and ground plate which leads to a rotation not constraint by the timber [19]. This leads to the compression and tension forces only being transferred by the rods. In the case shown in Figure 1 it shows a direct contact between the timber and steel which leads to a rotational restraint. The rotational axis with this restraint is not located in the center of the cross-section. The compressive material used is timber while the tensile material is steel, these materials have different elasticity moduli and dimensions. The differing elasticity moduli and size of the surfaces of the compressive and tensile zone causes the neutral axis to be off-center to guarantee a horizontal equilibrium, $\sum H = 0$, within the cross-section, this has been explored in Xu et al. [29]. The internal forces determined via the shifted neutral axis can be used to determine the rotational stiffness via a component model as seen in Yang [30] and are used for a prediction of the ultimate strength of the GiR connection.

https://doi.org/10.52202/080513-0180

2.3 TENSILE BEHAVIOUR OF GLUED-IN-RODS

The internal tensile force caused by the applied bending moment can yield different types of failure mechanisms of the glued-in-rods. Failure modes are often defined by the characteristics surrounding the failure, with GiR these are defined by the brittleness or ductility of the GiR connection and the location where the failure occurred [10].

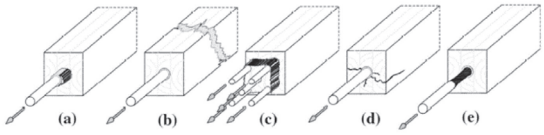

Figure 5: Possible failure mechanisms, (a) shear failure along the rod, (b) tensile failure, (c) shear block failure, (d) splitting failure, (e) yielding of the rod, Tlustochowicz et al. [27]

The mechanisms within Figure 5 can be divided into brittle (a), (b), (c), (d) and ductile (e) failure mechanisms. The brittle failure mechanisms (b) and (c) can be influenced by the design of the center to center distance between the rods and the diameter of one rod. Which one of the mechanisms (a), (d), and (e) occurs is dependant on the pull-out resistance and the yield capacity of the rod. The wanted failure mechanism depends on the wanted ductility of the connection, failure mechanism (e) is found to be the more ductile mechanism [19], [4]. In this research there is a focus on finding the maximum design strength capacity and rotational stiffness of the connection, it was opted to design for failure by mechanism (a) or (d). To test which way of failure is more dominant, the pull-out capacity is determined via predictions using Steiger et al. [23] and a working version of new generation Eurocode 5 [5]. This prediction is used in the design of an experimental test setup to see which failure mechanism can be expected and to determine the slip modulus of the connection.

2.4 NEUTRAL AXIS BEHAVIOUR

As mentioned in Subsection 2.2 the neutral axis is not located in the geometrical center of the cross-section. This is due to the non-homogeneity of the materials which represent the compressive and tensile part of the section. Methods to find the neutral axis are proposed in Ogrizovic [18] and Xu et al. [29], the latter finds that placing the timber directly on the steel plate increases the capacity due to the contribution of the compressive zone of the timber. The distance from the position of the internal forces to the neutral axis determines the moment capacity. Thus a shift of this neutral axis influences the moment capacity drastically. To find the position of the neutral axis a value has to be found where the contribution of the internal forces are equal on the respective compressive and tensile zone, this is treated in Chapter 3.

2.5 CROSS-SECTIONAL COMPOSITION

In order to design a cross-section considering the possible total moment on a structure which spans a road, a bigger cross-section is needed to resist the wind loading due to this connection being the determining factor for the design. Using four ”engineered timber products” as mentioned in Chapter 1 a Hollow Square Section (HSS) is produced out of these elements to ensure an equal moment resistance regardless of direction. To design this section the cross-section of the project in Naaldwijk found in Figure 1 was used. This section consists of 20 glued-in-rods in a HSS, the other parameters of the connection that are redesigned for this project are discussed in the next chapters. For the purpose of manufacturing a GL24h Spruce wood is chosen as the timber material. The first parameter is the rod diameter, which strongly influences the ductility and the tensile strength of the connection as yielding of the steel can become a failure mechanism when the rod diameter is smaller. In the case of seismic events where a ductile connection is wanted [18], [19] it can be seen that a smaller diameter or a lower strength steel leads to yielding of the steel and a more ductile behavior [4] instead of the brittle pull-out failure mechanisms. In other papers [3], [6] no clear direct relation was found between the actual pull-out strength and rod diameter. The rod diameter however does have a positive effect on the pull-out capacity of the GiR connection [27] due to the increased circumference of the rod. This increased circumference decreases the shear stress at the rod / adhesive interface, which decreases the chance of failure. In the project seen in Figure 1 a design capacity of 266.5 kNm is considered, using this value as input for the calculation methods mentioned in the Step1995 [25] or the method mentioned in Steiger et al. [23]. The result using M16-8.8 rods yields a unity check of approximately 1.0, for this reason it was chosen to create the cross-section with M16 rods with a steel quality of 8.8.

Having established the rod diameter, multiple design approaches can be taken with relation to geometrical properties such as glued-in depth, edge distance and relative distances. O’Neill et al. [17] defines the optimum glued in depth as 23.33 times the diameter and the optimum edge distance under combined bending and axial loading as 3.5d. The Step1995 [25] defines the edge distance as 4d, it was opted to test the edge distance mentioned in O’Neill et all [17]. The center to center distance is defined as the minimum distance where the group effect of the rod has no effect, which is 5 times the diameter as defined in Tlustochowicz et all [27] and Blass et all [1]. The considerations result in the cross-section seen in Figure 6. The cross-section is slightly modified to ensure it can be manufactured using slats of 40 mm thickness in the GLT.

3 – ANALYTICAL MODEL

To analytically determine the ultimate moment- and rotational capacity of a GiR connection, a model is created to calculate the position of the neutral axis. This model uses the pull-out capacity of a GiR rod and the number of rods below the neutral line of the cross-section, elasticity moduli, compressive strength and surfaces related to the compressive and tensile zones. The strength model is directly coupled to the neutral axis position model, a simple variant with one row of rods is explained as a step up to the model of the cross-section seen in Figure 6. In a similar manner a component model to predict the stiffness is composed.

https://doi.org/10.52202/080513-0180

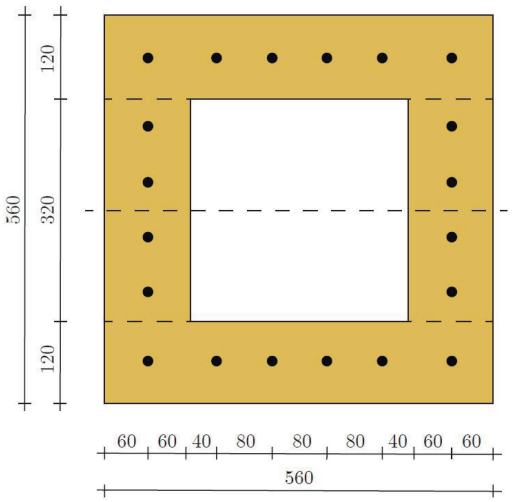

Figure 6: Final Cross-section

3.1 STRENGTH MODEL

Two assumptions were made to create this model. The first being that the cross-section remains plane. The second is that only the steel rods add to the tensile capacity of the internal forces. Both models explained below are designed to find the internal force equilibrium for the number of rod layers and surfaces present, this is visualized in equation (1).

$$\sum F_{compression} = \sum F_{tension} \tag{1}$$

3.1.1 Simple Geometry model

The simple model consists out of a square section of 560x560mm with a row of six steel rods at the bottom located at 60mm from said bottom, all sizes and distances are based on the cross-section of Figure 6. In Figure 7 a simplified version with a stress and strain distribution is shown.

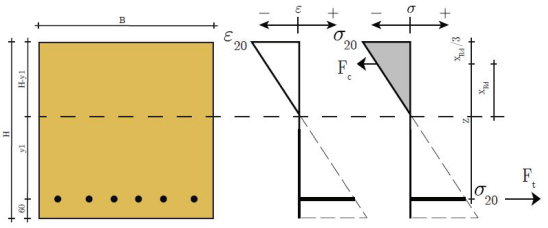

Figure 7: Cross-section with strain and stress distribution

As seen in equation (1) the internal force equilibrium has to be present. Both sides of this equation are rewritten in terms of the strain, this is done because in the linear-elastic phase, the strain is linear along the cross-section.

$$\sum F_c = \frac{(H - y_1) \cdot B \cdot E_{timber} \cdot \epsilon_{timber}}{2} \tag{2}$$

$$\sum F_t = A_{steel} \cdot E_{steel} \cdot \epsilon_{steel} \tag{3}$$

In equation (2) the resultant force F_c is described as the height of the compressive zone multiplied by the width of said zone divided by 2. This makes up the surface of the triangle seen in Figure 7. The surface is multiplied by the Modulus of Elasticity and the strain of the timber. In Equation (3) the resultant force F_t is the stress, here described as the elasticity modulus of steel times the strain of the steel according to Hooke's law, times the surface of the rods. Using equation (1) gives:

$$\frac{2 \cdot A_{steel}}{(H - y_1) \cdot B} \cdot \frac{E_{steel}}{E_{timber}} = \frac{\epsilon_{timber}}{\epsilon_{steel}} \tag{4}$$

The elasticity modulus of steel over the elasticity modulus of timber can be expressed in a factor 'n' with n = $\frac{E_{steel}}{E_{timber}}$. Due to the triangular shape of the strain distribution of both sides and that the strain is linear means that this can be seen as having equal ratios which leads to the following equation.

$$\begin{aligned} \frac{\epsilon_{timber}}{H - y_1} &= \frac{\epsilon_{steel}}{y_1} \\ \frac{\epsilon_{timber}}{\epsilon_{steel}} &= \frac{H - y_1}{y_1} \end{aligned} \tag{5}$$

Combining equations (4) and (5), including the factor 'n' gives the following result:

$$\frac{2 \cdot A_{steel} \cdot n}{(H - y_1) \cdot B} = \frac{H - y_1}{y_1} \tag{6}$$

Reshuffling the equation and writing this in terms of y_1 yields:

$$y_1^2 - 2y_1 \cdot (H + \frac{n \cdot A_{steel}}{B} + H^2 = 0 \tag{7}$$

This equation can be solved using the 'ABC' formula. With the standard solution filled in, that gives:

$$\begin{aligned} y_1 &= \chi \pm \sqrt{(\chi - H) \cdot (\chi + H)} \\ with \;\; \chi &= H + \frac{n \cdot A_{steel}}{B} \end{aligned} \tag{8}$$

Now that the neutral axis position has been determined, this can be used to make a prediction with regard to the moment resistance of the cross-section. This is done by determining the tensile force and multiplying by the distance 'z' seen in Figure 7. The maximum internal strain can be found by filling out equation (3) which is being determined by Hooke's law as seen in equation (9).

$$\begin{aligned} \epsilon_{steel} &= \frac{\Delta L}{L} \\ \Delta L &= \frac{F_{t,0} \cdot L}{E \cdot A} \\ \epsilon_{steel} &= \frac{F_{t,0}}{E \cdot A} \end{aligned} \tag{9}$$

https://doi.org/10.52202/080513-0180

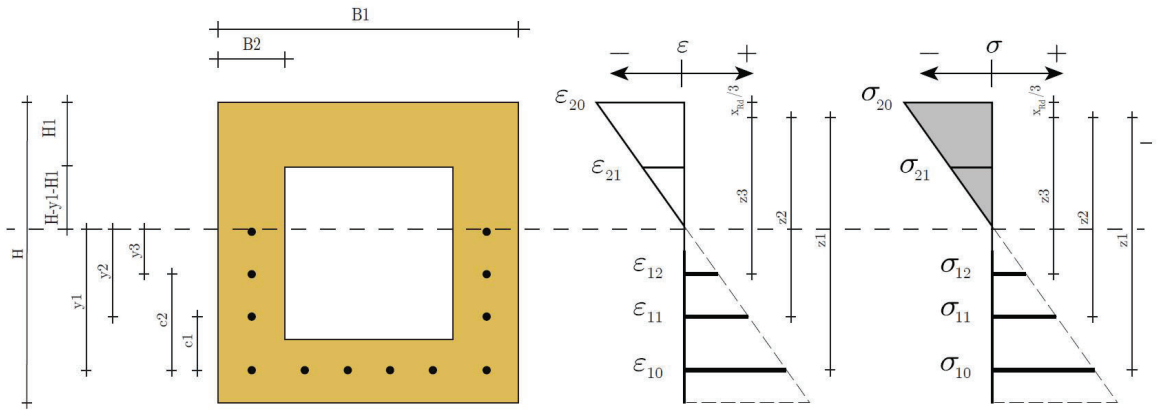

Figure 8: Complex cross-section with strain and stress distribution

With ' $F_{t,0}$ ' being the pull-out strength of the steel rod in the timber, F_t is later determined using experimental tests. Combining equations (3) and (9) leads to the conclusion that the internal tensile force is equal to 'number of rods (m)' · 'pull-out strength single rod (F_t)'. This is multiplied by 'Z' to give the following equation.

$$\begin{aligned} M &= m \cdot F_t \cdot Z \\ Z &= y_1 + \frac{2 \cdot (H - y_1)}{3} \end{aligned} \tag{10}$$

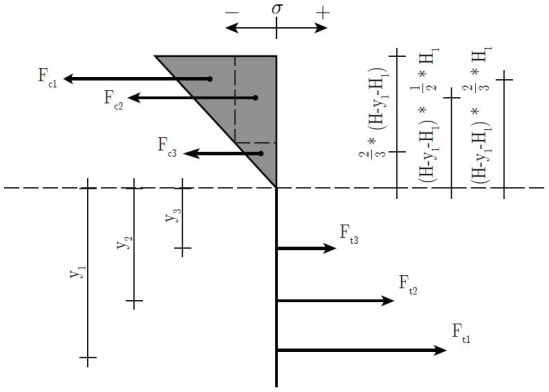

Figure 9: Complex cross-section internal force distribution with distances

3.1.2 Complex model

To determine the moment capacity for the complex cross-section as displayed in Figure 6 the same principles are used as in subsection 3.1.1. Since the same principles also apply the strain and stress distribution have a similar shape as seen in Figure 7. An overview can be found in Figure 8. Where y_i is the distance to the neutral axis of the i^{th} row of glued-in-rods. c_i is the distance of a row of rods relative to the bottom row of rods. B is the width of the cross-section. Where H is the height from the bottom row of rods to the top of the cross-section. In the Hollow Square Section (HSS) the tensile internal resulting force follows the same logic as in subsection 3.1.1. The compression zone is, however affected by the shape, the zone can be divided into three different resulting forces as can be found in Figure 9.

To fill out equation (1) the total force in the compressive and tensile area have to be determined. The respective compressive force can be stated as.

$$\begin{aligned} F_c =& F_{c1} + F_{c2} + F_{c3} \\ F_c =& \frac{1}{2} \cdot B_1 \cdot H_1 \cdot E_t y_1 (\epsilon_{20} - \epsilon_{21}) + \\ & B_1 \cdot H_1 \cdot E_t \cdot \epsilon_{21} + \\ & \frac{1}{2} \cdot 2 \cdot B_2 \cdot (H - y_1 - H_1) \cdot \epsilon_{21} \cdot E_t \end{aligned} \tag{11}$$

The strain ϵ_{21} can be expressed in terms of ϵ_{20} using the similar triangle method. The same procedure can be done for the internal tensile forces, which leads to the following equations.

$$\begin{aligned} F_t =& F_{t1} + F_{t2} + F_{t3} \\ F_t =& E_s \cdot A_s \cdot m_1 \cdot \epsilon_{10} + \\ & E_s \cdot A_s \cdot m_2 \cdot \epsilon_{11} + \\ & E_s \cdot A_s \cdot m_3 \cdot \epsilon_{12} \end{aligned} \tag{12}$$

Here is 'm' expressed as the number of rods in row number 'i', A_s is the surface of one rod and E_s is the modulus of elasticity of steel. The strains ϵ_{11} and ϵ_{12} can be expressed in terms of ϵ_{10} using the distances c and y_1, here similar triangles are used due to the linear distribution of the strain. Substituting said strains and the factor 'n' mentioned in subsection 3.1.1 while applying (1) using equations (11) and (12) gives a new equation. This equation is written in the same format as equation (4), combining this with equation (5) gives.

https://doi.org/10.52202/080513-0180

$$\frac{2A_s n(H-y_1)\cdot(-c_1\cdot m_2 - c_2\cdot m_3)+(m_1+m_2+m_3)\cdot y_1}{y_1\cdot(2B_2\cdot(-H+H_1+y_1)^2 - B_1H_1\cdot(-2H+H_1+2y_1))} = \frac{H-y_1}{y_1} \tag{13}$$

This equation can be solved for y_1 using the 'ABC' formula and the software program 'Mathematica', which gives two non-trivial solutions. Applying the criteria that $y_1 < H_1$ leaves only one solution, which is.

$$\begin{aligned} y_1 = {} & \frac{1}{4B_2}\cdot(4B_2\cdot H + 2B_1\cdot H_1 - 4B_2\cdot H_1 + \\ & 2A_s n(m_1+m_2+m_3) - ((4B_2H - 2B_1H_1 - \\ & 2A_s n(m_1+m_2+m_3))^2 - 8B_2\cdot(2B_2\cdot H^2 + \\ & 2B_1H_1H - 4B_2H_1H - B_1H_1^2 + 2B_2H_1^2 + \\ & 2A_s n\cdot(c_1m_2 + c_2m_3)))^{-\frac{1}{2}} \end{aligned} \tag{14}$$

This expression can be filled out using the parameters of any HSS with three rod layers below the neutral axis to find its position. This value finds the values of equations (11) and (12) using the internal strains. The positions of the internal forces and their magnitudes found in Figure 9 are used to find a resultant position for both the compressive and tensile side. The moment resisting capacity can be found using these positions and the magnitude of internal forces.

$$\begin{aligned} M &= Z_u \cdot \sum F_s \\ Z_u &= Y_{res} + X_{rd,resultant} \end{aligned} \tag{15}$$

4 – LABORATORY RESEARCH

The experimental research is divided into tests which determine material properties, as seen in subsections 4.1 and 4.2, and a four-point bending tests which measures the total moment capacity and rotation. The material properties test focus on the elasticity modulus of timber E_{timber} and the plastic compressive stress for the compressive tests. The pull-out test determines the slip modulus of a GiR k_{ser} and the pull-out strength N of a single rod. The culmination of variables found using the 'Compression' and 'Pull-out' tests are utilized to produce a numerical value from the Analytical model mentioned in Chapter 3. This value for the maximum internal moment is then compared to the results of an experiment using four-point bending test.

4.1 COMPRESSION TESTS

The compressive tests are performed in accordance with EN 408. The goal is to create a force-displacement diagram which is used to determine the elasticity modulus. The test setup contains a hydraulic press positioned above the sample. Two Linear Variable Differential Transformers (LVDTs) were placed on two opposite sides of the sample ranging from 30 percent to 70 percent along the length of the sample. There are two series used, one without a glued-in-rod (Series A) and one with a glued-in-rod (Series B). Both series have the exact same dimensions of 120x120x720 mm, which is a corner rod cut-out from the cross-section displayed in Figure 6. The glued-in-rod of Series B is located in the geometrical center of the cross-section of the sample. The tests are done with displacement control, EN 408 sets the displacement rate at 2 mm/min. The displacement rate is based on the guidelines, which specifies that tests should fail within 300 ±120 seconds.

4.2 PULL-OUT TESTS

The pull-out test is done in a pull-pull setup, meaning that there are GiRs glued in on both sides of the timber sample. An equal tensile force is applied to both rods, ensuring that the test setup is force-closed.

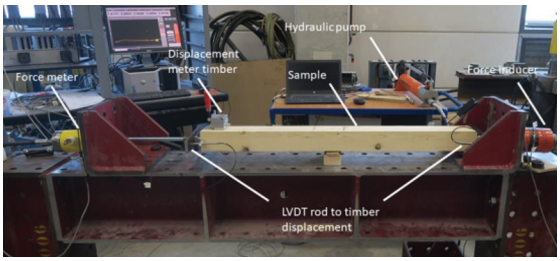

Figure 10: Test-setup pull-pull configuration

In Figure 10 the force hydraulic pump allows for a force-controlled test; the force is applied by pulling on both bars.

The LVDTs measure the displacement of the timber relating to the rod on both rods and opposite sides of the sample. The displacement meter of the timber measures the total timber elongation. The cross-section chosen is 80x120 mm with a 16 mm GiR located in the middle; this cross-section is a cut-out of the cross-section found in Figure 6, from one of the middle rods.

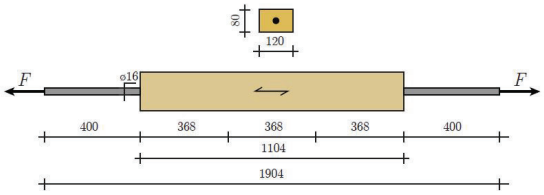

Figure 11: Pull-out test sample

The maximum force at which the steel rod yields, according to failure mechanism (e) displayed in Figure 5 is 100 kN. The brittle failure mechanisms of splitting and shear failure of the timber might occur before that value, for this reason a test speed of 15 kN/min was used.

4.3 FOUR POINT BENDING TEST

The test is done to measure the maximum moment capacity and rotational spring stiffness of the cross-section seen in Figure 6; the test is done in accordance with EN 408. The constant moment that this test provides makes a uniform test between the point of loading and the gluedin

https://doi.org/10.52202/080513-0180

depth. The analytical model can be used to estimate the capacity of this test after the compressive and pull-out tests are performed. There are three different measurements done, the vertical displacement is measured using lasers and Mitutoyo micrometers. The rotation using inclinometers at the center of the connection, and the shortening and lengthening of the compressive and tensile zones using LVDTs.

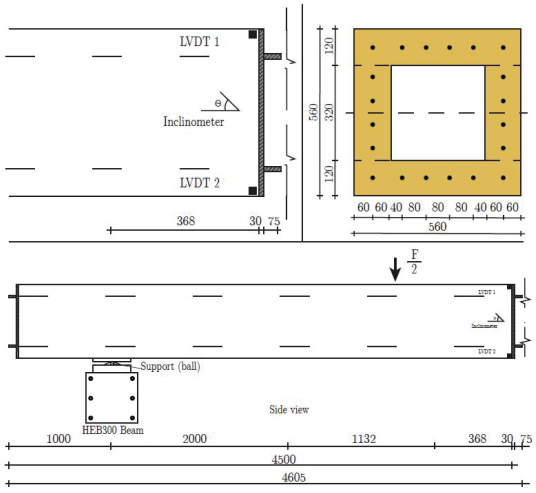

Figure 12: Four-point bending test setup

The figure shows half of the test setup, this setup is mirrored to create a force-closed system. The force is induced by a hydraulic press which is force-controlled using a pump, this force is divided into two using a steel beam to ensure equal force distribution in the four-point bending test. The introduction point of the force is located two meters from the support, causing the total moment to be equal to the total induced force.

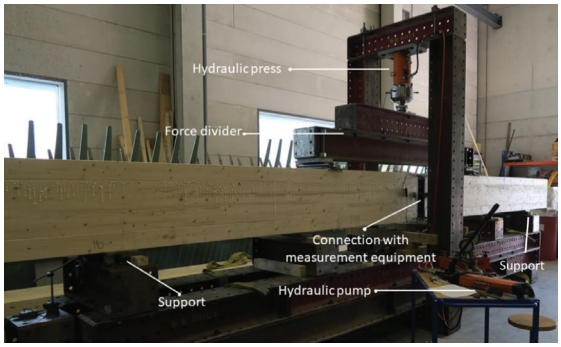

Figure 13: Four-point bending test picture

5 – RESULTS

The previously mentioned experimental investigation places a primary emphasis on the initial identification and determination of pertinent material parameters. These are subsequently employed as inputs for the proposed theoretical models. This section involves the results relating to the parameter experiments. After the parameter tests an examination of the theoretical model's performance in relation to empirical observations are derived from a four-point bending test conducted within the laboratory environment.

5.1 PARAMETER RESULTS

The parameter results relate to the compressive and pull-out tests.

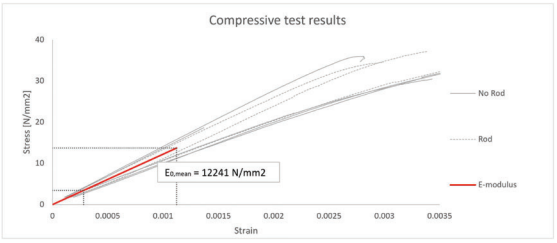

Figure 14: Results compressive tests

As found in Figure 14 it can be seen that the Series A and B samples have a negligible difference in terms of their stress capacity and Elasticity Modulus. The following results are extracted from the graph.

$$E_{0,mean} = 12\,241\ N/mm^2$$
$$\sigma_{c,0,mean} = 34.4\ N/mm^2 \tag{16}$$

The pull-out test results relate to the average pull-out strength and the slip modulus over the elastic trajectory.

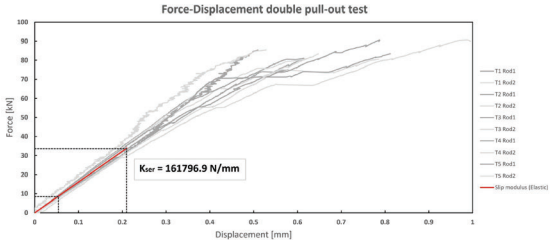

Figure 15: Results pull-out tests

In Figure 15 it can be seen that the beginning trajectory of the graph is similar amongst all tests, the failure capacity has a small variance in this series of experiments.

Table 1: Pull-out test results

	Capacity $F_{t,0}$ [kN]	Slip modulus K_{ser} [N/mm]
T1	85.4	164175
T2	80.6	168416
T3	81.0	173726
T4	90.7	147395
T5	83.4	159677
Average	84.2	161797

5.2 THEORETICAL MODEL IMPLEMENTATION

The results from the parameter experiments are used in the Complex model and Stiffness prediction as explained

https://doi.org/10.52202/080513-0180

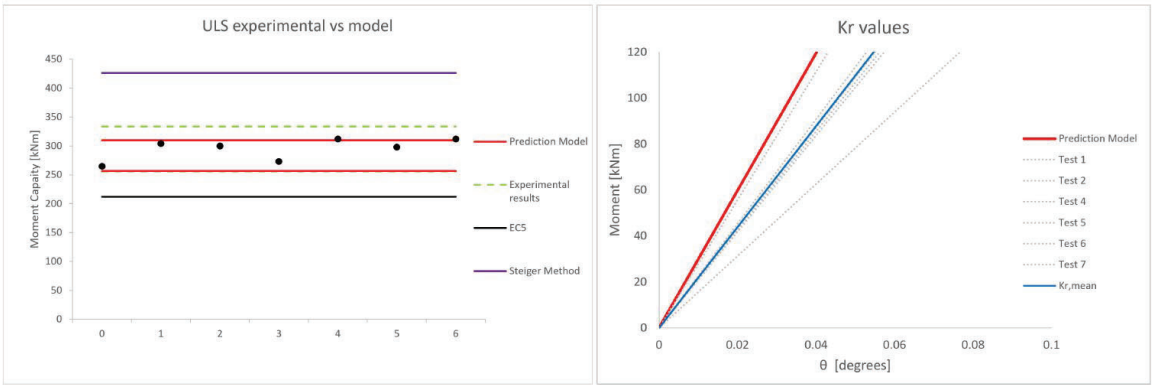

Figure 16: Strength and stiffness result comparison with theoretical models

in Chapters 3.1.2 and 3.2. The prediction for the moment capacity consists out of a lower and upper bound value, determined by the lower and upper bound value of the pullout strength, where the mean can be found in Table 1. The following results were determined.

Table 2: Prediction model results

y_1	315	mm
$F_{t,lower}$	76.3	kN
$F_{t,upper}$	92.1	kN
$M_{r,lower}$	255.8	kNm
$M_{r,upper}$	333.9	kNm
$K_{r,prediction}$	$1.71 \cdot 10^5$	kNm/rad

Beside the experimental tests of the pull-out capacity with a single rod there are also methods in literature to obtain this capacity. Two of these methods are found in the working version of the new Eurocode 5 [16] and in a paper by Steiger et all [23]. The results are found in the table below.

Table 3: Predicted Moment Capacity based on literature pull-out strengths

	Pull-out $F_{t,0}$ [kN]	Moment Capacity [kNm]
working version new EC5, characteristic	63.1	212.2
Steiger method, mean	126.7	426.1

These theoretical predictions are also compared to the experimental results.

5.3 FOUR-POINT BENDING TEST

The Four-Point bending test was performed six times, and since the leftover sample has a residual strength, there are seven results. The residual strength is the equivalent of the strongest failure in which the sample has participated. The two separate sides of the setup generate two results per side, a strength and a stiffness. The failure mechanism occurs as predicted on all six tests, the pull-out capacity of the rods was reached, an example of this can be found below.

Figure 17: Failure mechanism four point bending test

Table 4: Moment Capacity of the connection and comparison

	Moment Capacity [kNm]	EC 5 [%]	Seiger [%]
M1	265	+24.9	-37.8
M2	304	+43.3	-28.7
M3	300	+41.4	-29.6
M4	273	+28.7	-35.9
M5	312	+47.0	-26.8
M6	298	+40.4	-30.1
M7	312	+47.0	-26.8
$M_{r,k}$	256	+20.5	-40.0

The results relating to the experimental campaign can be found in the table above. Where the characteristic value of the working version of the new Eurocode 5 and the mean value via the Steiger method are compared to the prediction model based on their theoretical pull-out strength. The relative difference with the existing theoretical prediction methods is also displayed. These results are used to determine a lower and upper bound limit for the moment capacity, this combined with the theoretical predictions can be seen in Figure 16.

Looking at the capacity results of the test it can be noted that the variation coefficient of the results is relatively low at 6 percent. Furthermore it can be seen in the graph that the bottom boundary provided by the theoretical model corresponds with the experimental values. It can also be seen that the results of the prediction model, using the pull-

https://doi.org/10.52202/080513-0180

out capacity of either the working version of the new EC5 or the Steiger method, are inaccurate. The pull-out capacity of a single rod is overestimated in these current methods, causing the moment capacity to be severely overestimated.

5.4 ROTATIONAL STIFFNESS

To determine the rotational stiffness of the GiR connection from the displacement, the vertical displacement from the reference test is subtracted from the displacement of the test with the GiR connection. This is done over the 10 to 40 percent force trajectory of the test with connection. The rotational stiffness is determined using the following formula:

$$K_r = \frac{\alpha \cdot L}{4 \cdot \left(\frac{w_{con}}{F_{con}} - \frac{w_{ref}}{F_{ref}} \right)} \quad (17)$$

An overview of the rotational stiffness is found in the following table, the residual result does not contribute to the rotational stiffness result.

Table 5: Rotational Stiffness of the connection

	Rotational Stiffness K_r [kNm/rad]	$K_{r,prediction}$ [%]
M1	$8.96*10^4$	-47.7
M2	$1.25*10^5$	-27.2
M3	$1.39*10^5$	-19.0
M4	$1.20*10^5$	-30.0
M5	$1.59*10^5$	-6.9
M6	$1.22*10^5$	-28.6
$K_{r,mean}$	$1.26*10^5$	-26.6
$K_{r,theoretical}$	$1.71*10^5$	

In table 5 it is noted that the predicted value is an overestimation when compared to the experimental tests.

6 – DISCUSSION

Comparing the theoretical outcomes and experimental tests, it can be seen that the strength model provides accurate predictions. However, it must be noted that the stiffness prediction results in a 30 percent overestimation of the rotational stiffness of the GiR connection. This difference can be potentially attributed to the following factors. The stiffness prediction assumes perfect pull-out behaviour based on the pull-out capacity of a single rod. Due to the experimental setup, it is possible that the behaviour along the measured trajectory cannot be attributed solely to the tensile behaviour of the rod. Another assumption in the theoretical model is that the stiffness of the steel adapter is infinite, while in reality, this is not the case. These imperfections can also cause local effects in the deformation of the samples, these effects are not modelled within the stiffness prediction. Another problem encountered were the small measurements causing inaccuracies within the experimental results. An example of this would be the measurement of the angle using an inclinometer. The results, when plotted, had a large scatter due to the small value of the angle. These small values measured in the experiments appear to be inherent to this connection and cross-section, given its strong but brittle behaviour. This brittle behaviour also led to the sudden release of energy. When observing the samples after failure it can be observed that up until 5 layers of glued-in-rods are pulled out of the cross-section to varying distances. This means that the position of the neutral axis cannot be determined from the failed samples. The neutral axis was determined to activate three rows of rods in the tensile area of the cross-section and this is confirmed by the experimental strength results and its theoretical predictions. To gain a better statistical insight into the behaviour of the connection, more experiments should be conducted. In this paper the minimum number of experiments has been performed to ensure statistical viability. An increased number of experiments results in a smaller possible spread with regard to the moment capacity value.

7 – CONCLUSION AND RECOMMENDATION

In this research the moment capacity and rotational stiffness of a glued-in-rod connection was researched via analytical and experimental means. These results were also compared to existing theoretical prediction methods. It can be concluded that an accurate prediction model for the ULS capacity of said connection was written and that the connection fails in a consistent and expected manner. Once the pull-out strength is obtained a good estimation of the Moment capacity of this connection can be made. The current methods of predicting said pull-out strength are overestimating the actual capacity. Furthermore, a prediction was made with regards to the rotational stiffness of the connection, this has proven to be an overestimation of the experimental results. The proposed method should be expanded to gain a more comparative result. From all the experiments it can be concluded that this type of connection has a significant moment capacity but behaves in a very brittle manner. It is recommended to research the glue behaviour of said connection in more detail and see if a less brittle failure mechanism can be generated. Another recommendation would be further research into the prediction of the pull-out relating to a single GiR, so that the overestimation of the capacity can be reduced. Further research should also focus on the influence of changes in moisture content within the connection, this research could influence the mechanical behaviour of the proposed joint. Finally, this model should also be verified using multiple different geometries.

REFERENCES

[1] H. Blass and B. Laskewitz. *CIB - W18 meeting 32*. CIB, 1999.

[2] R. Bouchard, A. Salenikovich, C. Frenette, and G. Bedard-Blanchet. “Experimental investigation of joints with multiple glued-in rods in glued-laminated timber under axial tensile loading.” In: *Construction and Building Materials* 293 (2021), p. 122614.

[3] J. Broughton and A. Hutchinson. “Pull-out behaviour of steel rods bonded into timber.” In: *Materials and structures* 34 (2001), pp. 100–109.

https://doi.org/10.52202/080513-0180

[4] A. Buchanan, P. Moss, and N. Wong. "Ductile moment-resisting connections in glulam beams." In: *Proceedings of NZSEE conference, Wairakei Resort, Taupo, New Zealand*. 2001.

[5] CEN / TC 250 / SC 5 N 1615. *Eurocode 5 : Design of timber structures — Common rules and rules for buildings —Part 1-1 : General," pp. 235–244*. 2022.

[6] D. O. Chans, J. E. Cimadevila, and E. M. Gutiérrez. "Glued joints in hardwood timber." In: *International journal of adhesion and adhesives* 28.8 (2008), pp. 457–463.

[7] Dutch Government. *Climate change policy*. 2019.

[8] D. Flores, C. Dagenais, and P. Blanchet. "Characterizing the Performance of Adhesive Used in Glued-In Rod Timber Connections at Elevated Temperatures." In: *Journal of Performance of Constructed Facilities* 37.4 (2023), p. 04023035.

[9] F. P. I. for Forestry. *The Netherlands national market report 2021 presented to the UNECE committee*. Research Report. N. Services Probos Ministry of Agriculture, 2021.

[10] V. Gardelle and P. Morlier. "Geometric parameters which affect the short term resistance of an axially loaded glued-in rod." In: *Materials and structures* 40.1 (2007), pp. 127–138.

[11] N. Gattesco, A. Gubana, M. Buttazzi, et al. "Cyclic behaviour of glued-in-joints under bending moments." In: *Proc., 11th World Conf. on Timber Engineering (WCTE 2010)*. 2010, pp. 20–24.

[12] É. Gauthier-Turcotte, S. Ménard, M. Fiset, and W.-S. Chang. "Pull-out strength of glued-in steel rod perpendicular to the grain in spruce-pine glulam timber." In: (2021).

[13] P.-J. Gustafsson and E. Serrano. "Glued-in rods for timber structures-development of a calculation model." In: *TVSM-3000* TVSM-3056 (2001).

[14] G. Muciaccia. "An experimental approach to determine pull-out strength of single and multiple axially loaded steel rods bonded in glulam parallel to the grain." In: *Wood Material Science & Engineering* 14.2 (2019), pp. 88–98.

[15] S. Navaratnam, J. Thamboo, T. Ponnampalam, S. Venkatesan, and K. B. Chong. "Mechanical performance of glued-in rod glulam beam to column moment connection: An experimental study." In: *Journal of Building Engineering* 50 (2022), p. 104131.

[16] *NEN-EN 1995-1-1:2005+A2:2014+NB:2013 Hout - Algemeen*. NEN, 2020.

[17] C. O'Neill, D. McPolin, S. E. Taylor, T. Martin, and A. M. Harte. "Glued-in basalt FRP rods under combined axial force and bending moment: An experimental study." In: *Composite Structures* 186 (2018), pp. 267–273.

[18] J. Ogrizovic. "Post-Tensioned Timber Frames Under Wind and Seismic Loading." PhD thesis. ETH Zurich, 2019.

[19] J. Ogrizovic, R. Jockwer, and A. Frangi. "Seismic response of connections with glued-in steel rods." In: *INTER Proceedings: 2018 Tallinn, Estonia* 51 (2018), pp. 109–123.

[20] M. H. Ramage et al. "The wood from the trees: The use of timber in construction." In: *Renewable and sustainable energy reviews* 68 (2017), pp. 333–359.

[21] K. Raymakers. "Moment Resistant Column to Base Connection using Glued-in Rods in Glued Laminated Timber." Available at `https://pure.tue.nl/ws/portalfiles/portal/318193595/Raymakers_1253611_ABP_Moonen_MSc_thesis.pdf`. Master's thesis. Netherlands: Eindhoven University of Technology, 2023.

[22] Serano, E. *Glued-in-rods*. 2017.

[23] R. Steiger, E. Gehri, and R. Widmann. "Glued-in steel rods: a design approach for axially loaded single rods set parallel to the grain." In: *CIB-W18 meeting thirty-seven, Edinburgh, UK*. 2004.

[24] R. Steiger, E. Gehri, and R. Widmann. "Pull-out strength of axially loaded steel rods bonded in glulam parallel to the grain." In: *Materials and structures* 40 (2007), pp. 69–78.

[25] *STEP 1995. 1995, vol. 5, pp. 248–253*. Centrum Hout, 1995.

[26] J. Thamboo, S. Navaratnam, and T. Ponnampalam. "Pull-out resistance of glued in rod connection in timber: Reliability analyses using an experimental database." In: *Construction and Building Materials* 344 (2022), p. 128291.

[27] G. Tlustochowicz, E. Serrano, and R. Steiger. "State-of-the-art review on timber connections with glued-in steel rods." In: *Materials and structures* 44 (2011), pp. 997–1020.

[28] Trendeconomy. *Timber Import data*. 2022.

[29] B. Xu, A. Bouchaïr, and P. Racher. "Analytical study and finite element modelling of timber connections with glued-in rods in bending." In: *Construction and Building Materials* 34 (2012), pp. 337–345.

[30] H. Yang, W. Liu, and X. Ren. "A component method for moment-resistant glulam beam–column connections with glued-in steel rods." In: *Engineering Structures* 115 (2016), pp. 42–54.